Applied Physics Letters ARTICLE scitation.org/journal/apl

Microstructural heterogeneity drives reaction initiation in granular materials

Cite as: Appl. Phys. Lett. **114**, 254101 (2019); doi: 10.1063/1.5108902
Submitted: 3 May 2019 · Accepted: 10 June 2019 ·
Published Online: 24 June 2019

Joseph Bakarji[a] and Daniel M. Tartakovsky[a]

AFFILIATIONS

Department of Energy Resources Engineering, Stanford University, Stanford, California 94305, USA

[a]Authors to whom correspondence should be addressed: jbakarji@stanford.edu and tartakovsky@stanford.edu

ABSTRACT

Thermal localization leads to reaction initiation in granular materials. Observations show that it occurs in the vicinity of large pores and, thus, depends on a material's microstructure. Since the spatial variability of the latter cannot be ascertained in all its relevant details, we treat the material's initial porosity as a random field. The so-called "hotspots" are then modeled as rare events in a complex nonlinear dynamical system. Their probability of occurrence is quantified by the tails of the distributions of the temperature and the corresponding reaction rate. These are computed via Monte Carlo simulations of a two-phase five-equation dynamic compaction model, which are supplemented with a mesoscale model of the thermal localization at the solid-gas interface. Our results demonstrate a strong nonlinear dependence of the probability of hotspot initiation on the variance of the initial porosity.

Granular compaction has many important applications including processing pharmaceutical tablets,[1] metal powder consolidation,[2] diamond synthesis,[3] and energetic materials safety.[4] The behavior of reactive granular materials under dynamic compaction has been the subject of numerous experimental and theoretical studies.[5–8] The added complexity in understanding reactive powder mixtures lies in the need to model and predict thermal localization in critical areas of the material, known as "hotspots," where ignition occurs.

Although the physics of hotspots is not yet fully understood,[9] observations confirm the hypothesis that reaction initiation occurs in the vicinity of macropores.[10] This is consistent with the fact that areas with high plastic deformations cause large thermal dissipation and consequently extreme temperature fluctuations, which trigger chemical reactions. Other dynamic phenomena, such as shear banding[11] and elastoplastic deformation concentration due to material heterogeneities,[9] are also likely mechanisms contributing to hotspot formation. Furthermore, the grain size distribution has been shown to play a major role in the sensitivity of hotspot formation.[4]

In light of this knowledge, phenomenological[12] and computational[9] models of reaction initiation have been developed. The most common modeling approach is to use continuum models with thermodynamic closures and equations of state that are consistent with physics. Such continuum models account only for averaged microscopic dynamics, ignoring localization events that are due to microstructural defects. Since accurate physical measurements of reaction initiation are elusive, one has to rely on numerical modeling and simulation to study hotspot formation.

Hotspot formation in energetic materials has been extensively analyzed using (i) molecular dynamics simulations studying the thermochemical properties of hotspot formation, (ii) mesoscale pore collapse models of either a single pore or a few microstructural defects, characterizing the effect of the pore size and morphology on reaction initiation, and (iii) multiscale models that combine microscale dynamics with continuum models.

Molecular dynamic simulations[13,14] are essential to understand the underlying chemistry of hotspot formation. Yet, their computational cost renders them impractical for making quantitative predictions at the device scale.

Pore-scale numerical simulations have been used to characterize the criticality of hotspot formation.[10,15–17] The early work on isotropic (i.e., one-dimensional/radial) compaction of a viscoplastic spherical shell[18,19] has been extended to two- and three-dimensional simulations of a single macropore collapse.[15,20,21]

Multiscale simulations incorporate this mesoscale dynamics into continuum models by adding source terms, such as the phase pressure difference[8] or a reaction rate model,[22] to the latter. Another multiscale approach[23] is to build a surrogate model from multiple mesoscale pore collapse simulations and use it as part of a continuum scale simulation.

While the current trend in modeling hotspot formation is to incorporate as much physics as possible, the predictive uncertainty of

the resulting models (on any scale) is largely ignored. Specifically, continuum models are largely phenomenological and often neglect the subscale dynamics that is believed to be essential for hotspot formation. At any scale, models involve unknown parameters that are adjusted to fit experimental data, without necessarily reflecting the underlying physics. Although there is consensus that hotspots cause reaction initiation, they occur over wide time scales (10^{-5}–10^{-3} s), space scales (≈0.1–10 μm), and temperature ranges (≥700 K).[24] This makes it impossible to obtain accurate measurements and reliably validate a physical hypothesis. Consequently, many questions about modeling assumptions remain unanswered.

Is a single solid phase viscoplastic Euler model accurate enough to model granular compaction,[22,25] or is the gas phase essential for capturing the dynamics of hotspot formation?[26] Do closure terms in the two-phase models honor the underlying physics? Are equilibrium thermodynamic assumptions appropriate in a physical problem that is (clearly) very far from equilibrium? How accurate is the nonconservative compaction law in, e.g., the Baer-Nunziato model? Is the atomistic scale relevant in studying hotspot formation?

The absence of direct observational data does not allow one to discriminate between alternative modeling hypotheses and, hence, to answer conclusively these basic questions. For instance, two models might predict different temperatures and reaction rates, but be equivalent within a range of irreducible uncertainties. Thus, increasing modeling complexity and improving numerical accuracy do not necessarily improve the predictive power when the model parameters are uncertain.[27]

Yet, most material properties, e.g., porosity, pore size distribution, and heat capacity, are heterogeneous, and their point values are knowable only probabilistically. The values of some characteristics, such as viscosity and yield strength, are up to 100% uncertain in energetic materials like HMX.[9] Solid surface properties are usually assumed the same across the solid-gas interface, often without experimental validation.

These ubiquitous structural (model) and parametric uncertainties argue for the use of Occam's razor: A model that honors experimental observations with the fewest modeling assumptions is preferable. Guided by this principle, we show that treating initial porosity as random is sufficient to capture hotspot formation using a standard continuum model described below. The Monte Carlo solution of this problem reveals the high sensitivity of the probability of reaction initiation to the heterogeneity of initial porosity, which is consistent with experimental observations.

Two-phase (solid/gas) flow models[5,28] are widely used to describe the dynamics of a granular material under dynamic compaction (Fig. 1). In their original formulation, these seven-equation models combine conservation laws for mass, momentum, and energy in each phase with a nonconservative compaction equation for the volume fraction.[5] Subsequent studies provide simplified and regularized versions of the Baer-Nunziato equations,[6,29] found the relevant equations of state,[30–32] and added terms (e.g., "configurational stress") to account for the granular microstructure.[4,28] Despite their usefulness, these equations are known to be numerically unstable.

A single velocity/single pressure approximation[6] regularizes the equations and reduces the numerical instability.[33] The pressure-equilibrium assumption implies that the interface between the two phases is large. This five-equation model assumes the solid and gas

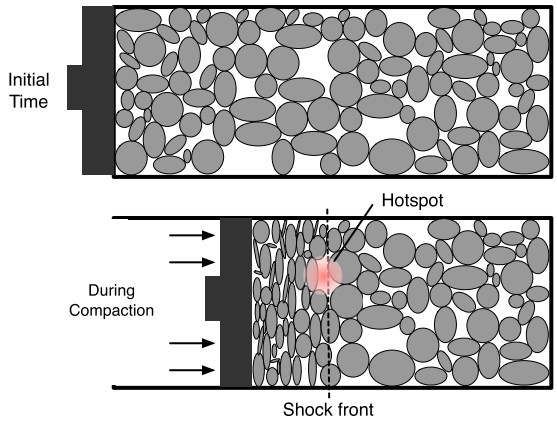

FIG. 1. Dynamic compaction of a granular material.

phases to have the same velocity u and pressure p, giving rise to four conservation equations

$$\text{Solid mass}: \quad \frac{\partial \alpha_s \rho_s}{\partial t} + \frac{\partial \alpha_s \rho_s u}{\partial x} = 0, \tag{1a}$$

$$\text{Gas mass}: \quad \frac{\partial \alpha_g \rho_g}{\partial t} + \frac{\partial \alpha_g \rho_g u}{\partial x} = 0, \tag{1b}$$

$$\text{Momentum}: \quad \frac{\partial \rho u}{\partial t} + \frac{\partial (\rho u^2 + p)}{\partial x} = 0, \tag{1c}$$

$$\text{Energy}: \quad \frac{\partial \rho E}{\partial t} + \frac{\partial (\rho E + p) u}{\partial x} = 0, \tag{1d}$$

where the subscripts s and g stand for the solid and gas phases whose densities are ρ_i ($i = s$ and g) and volume fractions are α_i ($i = s$ and g). The solid-gas mixture has density $\rho = \alpha_s \rho_s + \alpha_g \rho_g$, internal energy $e = \alpha_s \rho_s e_s + \alpha_g \rho_g e_g$ (with e_s and e_g denoting the internal energy of the solid and gas phases, respectively), total energy $E = e + B_s(\alpha_s) + u^2/2$ (with B_s denoting the configuration energy, a prescribed function of α_s, and the granular or configuration pressure defined by $\beta_s = \alpha_s \rho_s \mathrm{d}B_s/\mathrm{d}\alpha_s$), and pressure $p = \alpha_s p_s + \alpha_s p_g + \beta_s$ supplemented with the stiffened gas equation of state for the i-th phase $p_i = (\gamma_i - 1)\rho_i e_i - \gamma_i p_{i,\infty}$, where γ_i and $p_{i,\infty}$ are known material dependent constants. The fifth equation comprising the model is a nonconservative compaction law

$$\frac{\partial \alpha_s}{\partial t} + u \frac{\partial \alpha_s}{\partial x} = \frac{\rho_g c_g^2 - \rho_s c_s^2}{\rho_s c_s^2/\alpha_s + \rho_g c_g^2/\alpha_g} \frac{\partial u}{\partial x}. \tag{1e}$$

Hotspots are believed to occur in large pores where heat dissipation due to large plastic deformations and friction is the highest.[34] Therefore, the main quantity of interest (QoI) is the temperature at the solid/gas interface, rather than the average temperature $\bar{T}(x,t)$ that can be deduced from the internal energy of the continuum model (1). The mesoscale temperature, T_μ, is governed by a reaction-diffusion equation

$$\rho_s C_v \frac{\partial T_\mu}{\partial t} = \kappa \nabla^2 T_\mu + \dot{Q}_D + \dot{Q}_R. \tag{2}$$

The Laplacian $\kappa \nabla^2 T_\mu$ represents heat conduction into the solid bulk material. The rate of dissipation due to friction and permanent plastic deformation, $\dot{Q}_D$, is, e.g., given by the deformation power.[19] The

exothermal reaction heat generation term, $\dot{Q}_R$, follows an Arrhenius law.[12,22] In our analysis of hotspot formation, we focus on the dynamics before the onset of chemical reactions and neglect the reaction dissipation term $\dot{Q}_R$.

Our QoI is the pore-surface temperature $T_{\text{ps}}(x,t) = T_\mu(\mathbf{x}_{\text{sg}}, t)$, where $\mathbf{x}_{\text{sg}}$ is a point on the solid-gas interface. We expect that $T_{\text{ps}} \gg \bar{T}$, which can significantly change predictions of hotspot formation based on the continuum scale model. To account for the discrepancy between the continuum- and pore-scale temperatures, we adopt a reduced-order mesoscale heat model.[8] This model redistributes the macroscale temperature $\bar{T}(x,t)$ across the granular matrix by assuming a spherical shell mesoscale representation of the pores (Fig. 2).

The heat generated at the pore surface, q_c, depends on plastic deformation and, thus, on the rate of decrease in porosity $\partial\alpha_g/\partial t$. For spherical pores, $\alpha_g = \frac{4}{3}\pi R_g^3 N_g$, where R_g is the pore radius and N_g is the number of pores per unit volume. The heat generated at the surface dissipates into the bulk of the solid phase by heat conduction, q_s. The resulting temperature profile is given by the solution of the diffusion equation over a spherical shell. This gives the pore surface temperature[8]

$$T_{\text{ps}} = T_{\text{core}} + \beta_s \frac{\delta - R_g}{\lambda_s n} \frac{\partial R_g}{\partial t}, \tag{3}$$

where λ_s is the thermal conductivity and the parameter n determines the shape of the temperature profile. The heat dissipation boundary layer δ is determined from the average temperature constraint $\bar{T} = 1/V \int_{R_g}^{\delta} T \mathrm{d}V$ (Fig. 2). The core temperature T_{core} is determined from the solid-phase Hugoniot relation

$$e_s(p_s, \nu_s) - e_s^0(p_s^0, \nu_s^0) + \frac{p_s + p_s^0}{2}(\nu_s - \nu_s^0) = 0,$$

where $\nu_s = 1/\rho_s$ and the superscript 0 denotes the preshocked state.

An alternate measure of the probability of reaction initiation is the reaction rate $\dot{R}$ related to the pore surface temperature T_{ps} via the Arrhenius rate law[4]

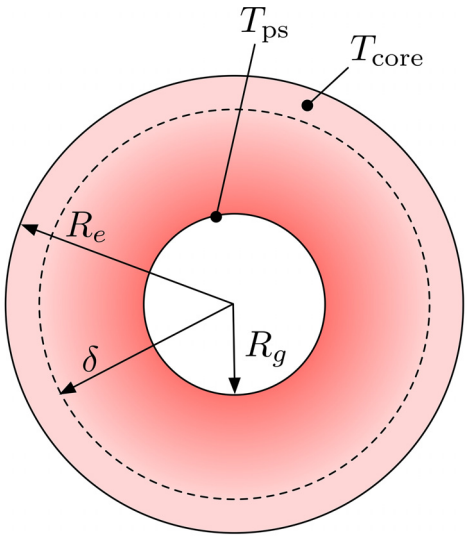

FIG. 2. Mesoscale spherical pore heat model.

$$\dot{R} = \left(1 - \frac{\alpha_s \rho_s}{\rho}\right) Z \exp\left(-\frac{T^*}{T_{\text{ps}}}\right) \tag{4}$$

where the exponential prefactor Z and the activation temperature T^* are known for a given material; they are set to $Z = 5 \times 10^{-19}$ s^{-1} and $T^* = 2.65 \times 10^4$ K in our simulations.[4] In this study, this quantity measures the "potential" average number of reactions triggered per unit time, without actually having reactions to take place. This assumes that the expected number of reactions per unit time is directly related to the probability of initiation at each point (x, t).

Microstructural heterogeneity in granular materials is the source of (i) fast temperature and stress fluctuations in the vicinity of large pores and (ii) an epistemic uncertainty in the key pore size and material property distribution. Accordingly, we treat the initial porosity, $\alpha_g(x, t = 0)$, as a spatially uncorrelated Gaussian random field, $\alpha_g(x, 0) \sim \mathcal{N}(\bar{\alpha}_g, \sigma_g^2)$, such that

$$\langle \alpha_g \rangle = \bar{\alpha}_g, \quad \langle \alpha_g(x', 0)\alpha_g(x, 0) \rangle = \sigma_g^2 \delta(x' - x), \tag{5}$$

where $\langle \cdot \rangle$ denotes the ensemble average. This approximation is valid for randomly packed grains with no spatial correlation at the grid size ($\sim 10\,\mu$m). Spatially correlated microstructures inferred from real images can also be used.

We use (1)–(3), subject to this random initial condition, to estimate the probability of pore-surface temperature $T_{\text{ps}}(x,t)$ exceeding a reaction initiation threshold T_{ig}

$$\begin{aligned} \mathbb{P}\left[T_{\text{ps}}(x,t) > T_{\text{ig}}\right] &= 1 - \mathbb{P}\left[T_{\text{ps}}(x,t) < T_{\text{ig}}\right] \\ &= 1 - \mathscr{F}_{T_{\text{ps}}}(T_{\text{ig}}; x, t), \end{aligned} \tag{6}$$

where $\mathscr{F}_{T_{\text{ps}}}$ is the cumulative distribution function (CDF) of the random surface temperature $T_{\text{ps}}(x,t)$. We start by assuming that reactions are instantaneously triggered when T_{ps} exceeds the known threshold T_{ig}, which represents a zeroth-order approximation of the probability of reaction initiation.

We use Monte Carlo simulations to estimate these probabilities. In every realization, (1)–(3) are solved with the initial condition $\alpha_g(x, 0)$ drawn from the distribution $\mathcal{N}(\bar{\alpha}_g, \sigma_g^2)$ at every grid-point with no spatial correlation. The simulation domain of length 1.6 cm is discretized with 200 grid points, and $N_r = 600$ realizations were performed. Every realization i yields a pore-surface temperature $T_{\text{ps}}^i(x,t)$. The ensemble average is approximated by the sample average $\langle T_{\text{ps}} \rangle \approx \langle T_{\text{ps}} \rangle_{\text{s}} = \sum_i T_{\text{ps}}^i / N_r$, and the probability density function is constructed using a kernel density estimator $f_{T_{\text{ps}}}(\hat{T}; x, t) \approx \sum_i K_h(\hat{T} - T_{\text{ps}}^i(x,t))/N_r$, where $\hat{T}$ is a sample space variable and $K_h(\cdot)$ is a Gaussian kernel with bandwidth h.

A Godunov-type HLLC numerical scheme[33] is used, with a velocity boundary condition, $v_p \approx 60$ m/s, on the left boundary (Fig. 1) and a reflecting boundary condition on the right (although the simulation is stopped right before the shock reaches that boundary). The nonconservative and highly nonlinear nature of the compaction law (1e) requires special treatment to preserve the volume fraction positivity.

Figure 3 shows a snapshot of one realization of the two main variables at time $t = 12\,\mu$s: the solid volume fraction $\alpha_s(x, \cdot)$ and the pore surface temperature $T_{\text{ps}}(x, \cdot)$. The temperature is higher, particularly at the shock front, for a higher microstructural heterogeneity corresponding to a larger σ_g. Comparison of the gas volume fraction before

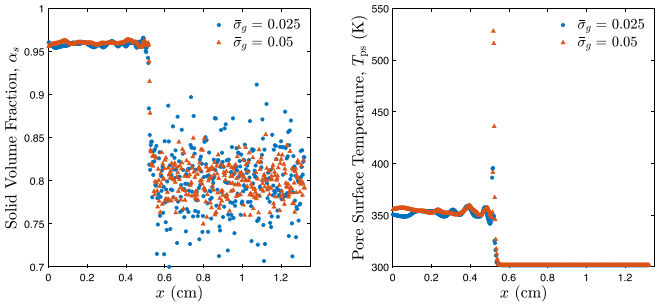

FIG. 3. Spatial profiles of the solid volume fraction α_s (left) and pore-surface temperature T_{ps} (right) at time $t = 34$ μs, for two values of the microstructural fluctuation strength σ_g.

and after the shock reveals that once the grains are compressed, the porosity becomes relatively homogeneous. Hence, larger pores deform more than smaller ones, thus dissipating more energy. This is consistent with experimental observations.[9]

The average pore-surface temperature $\langle T_{ps} \rangle_s$ is almost independent of the initial microstructural heterogeneity σ_g (Fig. 4, left). However, the average reaction rate $\langle \dot{R} \rangle_s$ increases with σ_g (Fig. 4, right). The increased sensitivity of $\langle \dot{R} \rangle_s$ to σ_g is due to the nonlinearity of the Arrhenius law, which gives exponentially higher weights to higher temperatures.

Both the average pore-surface temperature $\langle T_{ps}(x,t) \rangle_s$ and the average reaction rate $\langle \dot{R} \rangle_s$ are the highest along the line $x/t = v_{sh}$, where v_{sh} is the speed of the shock (Fig. 5). This is because the highest rate of thermal generation occurs where the change in porosity is the highest. Behind the shock front, the temperature decreases due to thermal diffusion in the bulk.

Figure 5 shows the average reaction rate and pore surface temperature. The line with the peak reaction rate and pore surface temperature coincides with the shock front where plastic deformations are the highest. The average temperature behind the shock front is higher than the initial temperature due to the increase in pressure after compaction (also see Fig. 3). Temperature fluctuations cause the reaction rate to grow exponentially due to the Arrhenius law. This explains the fluctuations in the sample mean of the reaction rate, which amplify rare extreme temperature fluctuations that are averaged out in $\langle T_{ps} \rangle_s$. The impact of the increase in temperature behind the shock front is insignificant compared to that of extreme fluctuations.

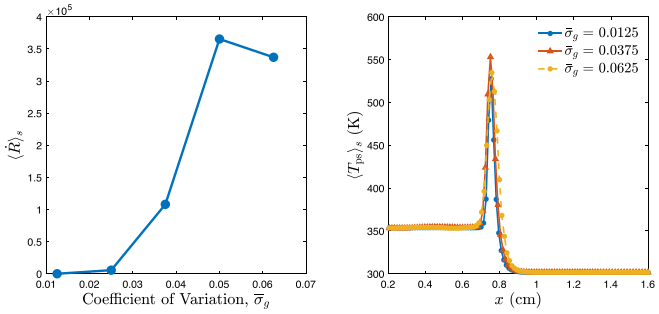

FIG. 4. Average temperature (right) and the corresponding reaction rate (left) as a function of microstructural heterogeneity σ_g.

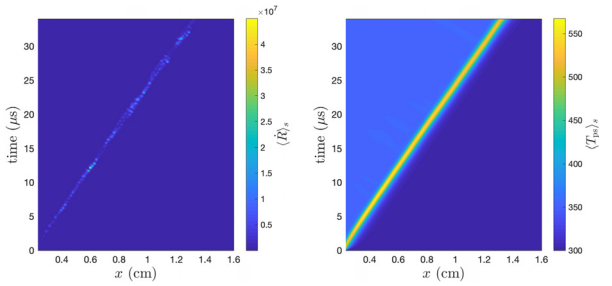

FIG. 5. Average reaction rate $\langle \dot{R} \rangle_s$ (left) and average pore-surface temperature $\langle T_{ps} \rangle_s$ (right), for the coefficient of variation $\bar{\sigma}_g = 0.0375$.

We posit that the reaction initiation occurs when the temperature T_{ps} exceeds a certain threshold T_{ig} and computing the probability of this event, $\mathbb{P}[T_{ps}(x,t) > T_{ig}]$ using (6). This probability is shown in Fig. 6 as a function of T_{ig} (left) and $\bar{\sigma}_g$ (right), for an arbitrary point (x_h, t_h) along the shock front (chosen for illustration). This observation highlights the fact that hotspots are not a function of the average pore surface temperature, but of the tail of the distribution. Furthermore, the dependence on T_{ig} confirms the intuition that the probability of initiation increases as the ignition threshold is lowered, thus becoming easier to exceed.

The exceedance probability in Fig. 6 provides a partial description of the probability of reaction initiation. Another relevant statistics is the probability of T_{ps} remaining above the ignition threshold T_{ig} for a certain time interval $\tau = t_2 - t_1$ that is sufficient for the reactions to take hold. In other words, we are concerned with the probability of $T_{ps} > T_{ig}$ during a given time interval τ: $\mathbb{P}[T_{ps}(x,t_1) > T_{ig}, T_{ps}(x,t_2) > T_{ig}] = \mathscr{F}_t[\tau | T_{ps} > T_{ig}]$, for all x and all permutations of t_1 and t_2. The corresponding CDF in Fig. 7 shows that the time interval during which temperature T_{ps} remains above the threshold T_{ig} increases with the microstructural fluctuation coefficient of variation $\bar{\sigma}_g$.

In summary, we demonstrated the dependence of reaction initiation in compacted granular materials on the initial pore size distribution using a fluctuating initial microstructure. Our results show that the amplitude of the fluctuations in the initial porosity affected the distribution of the resulting pore-surface temperature, motivating a probabilistic approach to studying hotspot formation. The corresponding reaction rate and probability of initiation are sensitive to the

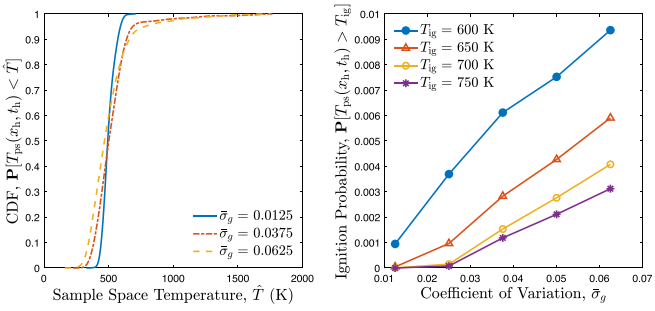

FIG. 6. CDF of a random pore-surface temperature T_{ps} at a given point along the shock front (x_h, t_h) (left). Probability of reaction initiation as a function of the strength of microstructural fluctuations σ_g for different ignition temperatures T_{ig} (right).

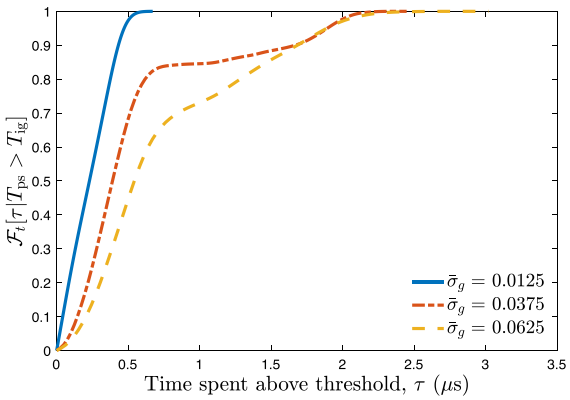

FIG. 7. Probability density function of the time spent above the reaction initiation threshold, for a 34 μs simulation.

fluctuation amplitude. This study demonstrates that a probabilistic approach is the simplest and most intuitive way to study reaction initiation in granular materials, given a fundamentally uncertain and spatially heterogeneous material microstructure.

REFERENCES

[1]F. X. Sanchez-Castillo, J. Anwar, and D. M. Heyes, "Molecular dynamics simulations of granular compaction," Chem. Mater. **15**, 3417–3430 (2003).
[2]T. J. Vogler, M. Y. Lee, and D. E. Grady, "Static and dynamic compaction of ceramic powders," Int. J. Solids Struct. **44**, 636–658 (2007).
[3]O. G. Epanchintsev, A. S. Zubchenko, A. E. Korneyev, and V. A. Simonov, "Highly-efficient shock-wave diamond synthesis from fullerenes," J. Phys. Chem. Solids **58**, 1785–1788 (1997).
[4]J. B. Bdzil, R. Menikoff, S. F. Son, A. K. Kapila, and D. S. Stewart, "Two-phase modeling of deflagration-to-detonation transition in granular materials: A critical examination of modeling issues," Phys. Fluids **11**, 378 (1999).
[5]M. R. Baer and J. W. Nunziato, "A two-phase mixture theory for the deflagration-to-detonation transition (ddt) in reactive granular materials," Int. J. Multiphase Flow **12**, 861–889 (1986).
[6]A. K. Kapila, R. Menikoff, J. B. Bdzil, S. F. Son, and D. S. Stewart, "Two-phase modeling of deflagration-to-detonation transition in granular materials: Reduced equations," Phys. Fluids **13**, 3002–3024 (2001).
[7]D. Eakins and N. N. Thadhani, "The shock-compression of reactive powder mixtures," Int. Mater. Rev. **54**, 181–213 (2009).
[8]R. Saurel, F. Fraysse, D. Furfaro, and E. Lapebie, "Multiscale multiphase modeling of detonations in condensed energetic materials," Comput. Fluids **169**, 213–229 (2018).
[9]C. A. Handley, B. D. Lambourn, N. J. Whitworth, H. R. James, and W. J. Belfield, "Understanding the shock and detonation response of high explosives at the continuum and meso scales," Appl. Phys. Rev. **5**, 011303 (2018).
[10]C. M. Tarver, S. K. Chidester, and A. L. Nichols, "Critical conditions for impact- and shock-induced hot spots in solid explosives," J. Phys. Chem. **100**, 5794–5799 (1996).
[11]R. A. Austin, N. R. Barton, J. E. Reaugh, and L. E. Fried, "Direct numerical simulation of shear localization and decomposition reactions in shock-loaded HMX crystal," J. Appl. Phys. **117**, 185902 (2015).
[12]E. L. Lee and C. M. Tarver, "Phenomenological model of shock initiation in heterogeneous explosives," Phys. Fluids **23**, 2362–2372 (1980).
[13]S. W. Bunte and H. Sun, "Molecular modeling of energetic materials: The parameterization and validation of nitrate esters in the COMPASS force field," J. Phys. Chem. B **104**, 2477–2489 (2000).
[14]A. Strachan, E. M. Kober, A. C. T. Van Duin, J. Oxgaard, and W. A. Goddard III, "Thermal decomposition of RDX from reactive molecular dynamics," J. Chem. Phys. **122**, 054502 (2005).
[15]N. K. Rai and H. S. Udaykumar, "Void collapse generated meso-scale energy localization in shocked energetic materials: Non-dimensional parameters, regimes, and criticality of hotspots," Phys. Fluids **31**, 016103 (2019).
[16]N. K. Rai, M. J. Schmidt, and H. S. Udaykumar, "High-resolution simulations of cylindrical void collapse in energetic materials: Effect of primary and secondary collapse on initiation thresholds," Phys. Rev. Fluids **2**, 043202 (2017).
[17]G. A. Levesque and P. Vitello, "The effect of pore morphology on hot spot temperature," Propellants, Explos., Pyrotech. **40**, 303–308 (2015).
[18]M. M. Carroll and A. C. Holt, "Static and dynamic pore-collapse relations for ductile porous materials," J. Appl. Phys. **43**, 1626–1636 (1972).
[19]V. Nesterenko, *Dynamics of Heterogeneous Materials* (Springer Science & Business Media, 2013).
[20]L. Tran and H. S. Udaykumar, "Simulation of void collapse in an energetic material, Part I: Inert case," J. Propul. Power **22**, 947–958 (2006).
[21]N. K. Rai and H. S. Udaykumar, "Three-dimensional simulations of void collapse in energetic materials," Phys. Rev. Fluids **3**, 033201 (2018).
[22]O. Sen, N. K. Rai, A. S. Diggs, D. B. Hardin, and H. S. Udaykumar, "Multi-scale shock-to-detonation simulation of pressed energetic material: A meso-informed ignition and growth model," J. Appl. Phys. **124**, 085110 (2018).
[23]A. Nassar, N. K. Rai, O. Sen, and H. S. Udaykumar, "Modeling mesoscale energy localization in shocked HMX, Part I: Machine-learned surrogate models for the effects of loading and void sizes," Shock Waves **29**, 537–558 (2019).
[24]F. P. Bowden and A. D. Yoffe, *Initiation and Growth of Explosion in Liquids and Solids* (CUP Archive, 1985).
[25]D. S. Stewart, B. W. Asay, and K. Prasad, "Simplified modeling of transition to detonation in porous energetic materials," Phys. Fluids **6**, 2515–2534 (1994).
[26]P. Embidt, J. Hunters, and A. Majda, "Simplified asymptotic equations for the transition to detonation in reactive granular materials," SIAM J. Appl. Math. **52**, 1199–1237 (1992).
[27]M. Sinsbeck and D. M. Tartakovsky, "Impact of data assimilation on cost-accuracy tradeoff in multifidelity models," SIAM/ASA J. Uncertainty Quant. **3**, 954–968 (2015).
[28]R. Saurel, N. Favrie, F. Petitpas, M. H. Lallemand, and S. L. Gavrilyuk, "Modelling dynamic and irreversible powder compaction," J. Fluid Mech. **664**, 348–396 (2010).
[29]R. Saurel, S. Le Martelot, R. Tosello, and E. Lapébie, "Symmetric model of compressible granular mixtures with permeable interfaces," Phys. Fluids **26**, 123304 (2014).
[30]G. Baudin and R. Serradeill, "Review of jones-wilkins-lee equation of state," in *EPJ Web of Conferences* (EDP Sciences, 2010), Vol. 10, p. 00021.
[31]W. C. Davis, "Complete equation of state for unreacted solid explosive," Combust. Flame **120**, 399–403 (2000).
[32]S. Jolgam, A. Ballil, A. Nowakowski, and F. Nicolleau, "On equations of state for simulations of multiphase flows," in *World Congress on Engineering, 4–6 July, 2012* (International Association of Engineers, London, UK, 2012), Vol. 3, pp. 1963–1968.
[33]R. Saurel, F. Petitpas, and R. A. Berry, "Simple and efficient relaxation methods for interfaces separating compressible fluids, cavitating flows and shocks in multiphase mixtures," J. Comput. Phys. **228**, 1678–1712 (2009).
[34]R. Menikoff, "Compaction waves in granular HMX," AIP Conf. Proc. **505**, 397–400 (2000).